Laser Joining of CFRTS and Steel by Interfacial Pressure Control

The porosity in the CFRTS/steel joint was shown to be caused by the solidification shrinkage of the resin, resulting in a decrease in joint strength

BY J. BAI, S. YANG, Z. LIN, AND Q. YIN

Abstract

The carbon fiber-reinforced polymer (CFRP) metal structure is widely used in various industries to reduce the weight and cost of the structure without compromising performance. The main challenge for manufacturing the CFRP metal structure comes from the lack of flexible and robust joining processes. In this study, a new laser joining process was developed that used a thin layer of polyamide 6 as an interlayer material lying between carbon fiber-reinforced thermosets and a quenching-partition (QP) 980 steel to achieve the joint since the laser can't directly join the steel to the thermoset composite. It was found that the joint's strength was seriously degraded by the porosity's formation. The porosity formation mechanism was studied by online-recording the thermal history inside the joint during the laser joining process. Experimental results demonstrated that the emerging of the porosities in the joint was mainly caused by the cooling shrinkage instead of pyrolysis gas release. Furthermore, a new approach of controlling and optimizing the interfacial pressure was developed to suppress the porosity formation in the joint, which can significantly reduce the porosity rate from 25.8 to 1.2% and dramatically improve the joint shear strength from 10.69 to 18.6 MPa by 73.99%.

https://doi.org/10.29391/2022.101.022

Keywords

- Laser Joining
- Carbon Fiber-Reinforced Thermoset (CFRTS)
- CFRTS/Steel Hybrid Structures
- Porosity
- Fracture

Introduction

In recent years, with an increasing requirement of lightweight structures in various industries such as automotive, shipbuilding, and aerospace, carbon fiber-reinforced polymers (CFRPs) have been widely used due to their high strength and corrosion resistance (Ref. 1). More and more CFRP-metal hybrid joints have been applied to develop the comprehensive performance of various materials and reduce costs (Refs. 2, 3). Exploiting the reliable jointing technique of metal and CFRPs has become a popular research topic all over the world.

At present, mechanical joining and adhesive bonding are commonly used to join composites and metals. Joints made by mechanical joining, such as riveting and bolting, show very high joining strength. However, the containing holes will damage the continuity of the fiber, resulting in stress concentration around the hole and reduced strength and stability of the composite material (Ref. 4). In addition, the metal fasteners will increase the structural weight and accelerate electrochemical galvanic corrosion. Adhesive bonding has uniform load distribution, good sealing, and insulation. The main issue with adhesive bonding is its poor aging in service environments. In addition, adherent surfaces require special surface treatment and long curing cycles, which make the process more complicated (Refs. 5, 6).

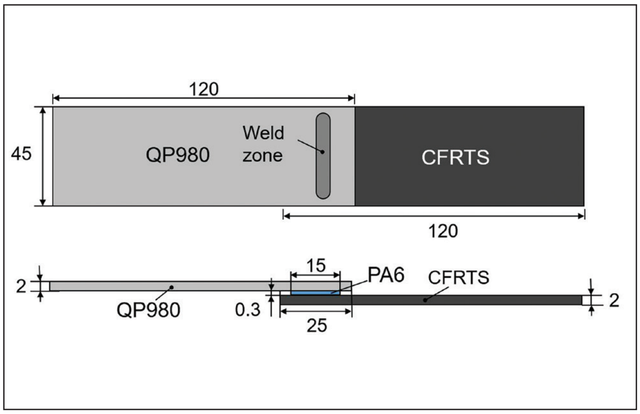

Fig. 1 — Sample size and lap joint diagram.

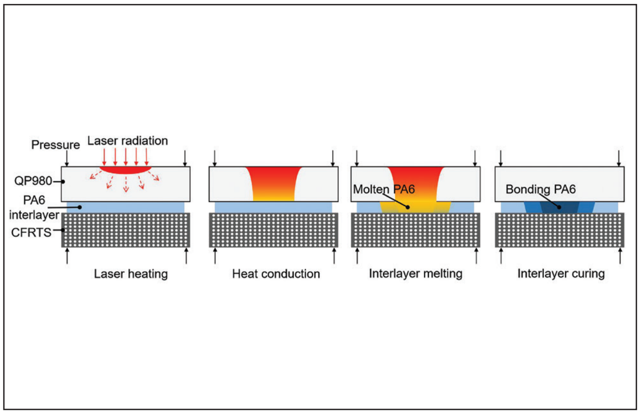

Fig. 2 — QP980/CFRTS laser joining process.

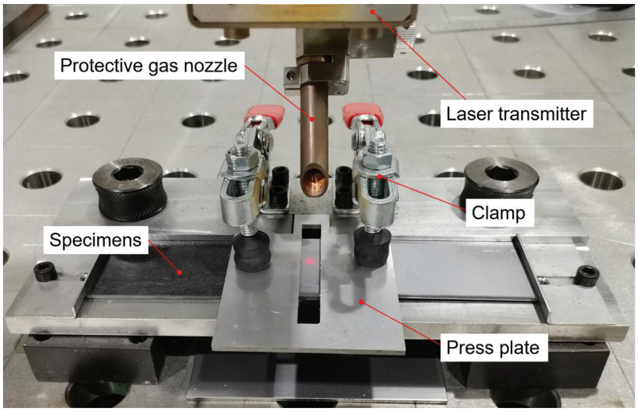

Fig. 3 — Laser joining experiment setup.

With its high efficiency, high flexibility, accessibility, and no weight gain, laser welding has become the focus of attention in various application fields (Refs. 2, 6). In recent years, researchers around the world have made a series of gains in laser joining carbon fiber-reinforced thermoplastic (CFRTP) and metal materials. Jung et al. (Refs. 1, 4, 5) have joined CFRTP to galvanized steel, stainless steel, and aluminum alloy by laser-assisted direct joining. The ultimate shear forces of the lap joint were 3300N, 4800N, and 3000N, respectively. Current research mainly focuses on the laser joining between CFRTP and metal materials, but there is little research on laser joining between carbon fiber-reinforced thermosets (CFRTSs) and metal. The main reason is CFRTSs can't be melted twice and directly joined with metals. CFRTSs are more widely applied due to their low cost, considerable high temperature stability, and flame retardancy. Therefore, the study of laser joining between CFRTSs and metal is of great significance. Lin et al. (Ref. 6) investigated the feasibilities, characteristics, and mechanisms of the laser heterogeneous jointing of a CFRTS and dual-phase steel (DP590) with the aid of an intermediate polycarbonate (PC) mid-layer. They found that the joint strength was higher when a fracture occurred in the mid-layer or a CFRTS resin base plate. The research shows that the CFRTS and steel both interlocked mechanically with the PC mid-layer, resulting in a shear strength of 4.9 MPa. Previous experimental results showed that the strength of the joint produced by laser joining was generally lower than that by mechanical joining or adhesive bonding.

The internal porosity of the joint is a detrimental factor seriously affecting the joint strength of the CFRP/metal joint. Chen et al. (Ref. 7) found that the formation of bubbles in the joint zone of Ti/PET sheets was inevitable, and the number of bubbles increased with the increase of laser power. Tan et al. (Ref. 8) revealed that there are two types of porosities in the CFRTP/steel joint. One was caused by the resin pyrolysis gas, such as CO_2, NH_3, H_2O, and hydrocarbons. The other type was produced by the shrinkage of melted CFRP in the solidification stage. Lin et al. (Ref. 6) reported that pyrolysis of epoxy resin or PC resulted in gases such as CO_2, CO, CH_4, and H_2O, which entered the molten PC and generated bubbles. Although some studies have shown that the high pressure generated by pyrolysis gas can enhance the connection of the interface between the thermoplastic and metal (Refs. 2, 4, 6), the porosity reduces the payload area and results in stress concentration, leading to joint fracture in the porosity area within the thermoplastic. Therefore, eliminating the porosities during laser joining is the key to improving the mechanical properties of the joint. However, the mechanism of the porosity formation in the CFRTS/metal joint with the aid of an interlayer has not been verified, and an efficient strategy to suppress the formation of these porosities is lacking. It is important to clearly understand the internal porosity formation mechanism and develop a new approach to successfully achieve high-quality CFRTS/metal joints.

In this study, polyamide 6 (PA6) was adopted as an interlayer lying between the CFRTS and QP980 steel to laser join them. The mechanism of the porosity formation was explored by online-recording a thermal history inside the joint, in which the formation of these porosities was confirmed to be caused by molten PA6 shrinkage during the cooling and solidification stages. Furthermore, the optimized interfacial pressure of QP980/CFRTS can compress the molten PA6 and inhibit the shrinkage defects. The porosity rate was significantly reduced from 25.8 to 1.2%, and the fracture mode of QP980/CFRTS joints was changed from the cohesive fracture of PA6 interlayer to the interface fracture of QP980/PA6. Therefore, the shear strength of the CFRTS and QP980 steel joint was dramatically increased from 10.69 to 18.6 MPa by 73.99%.

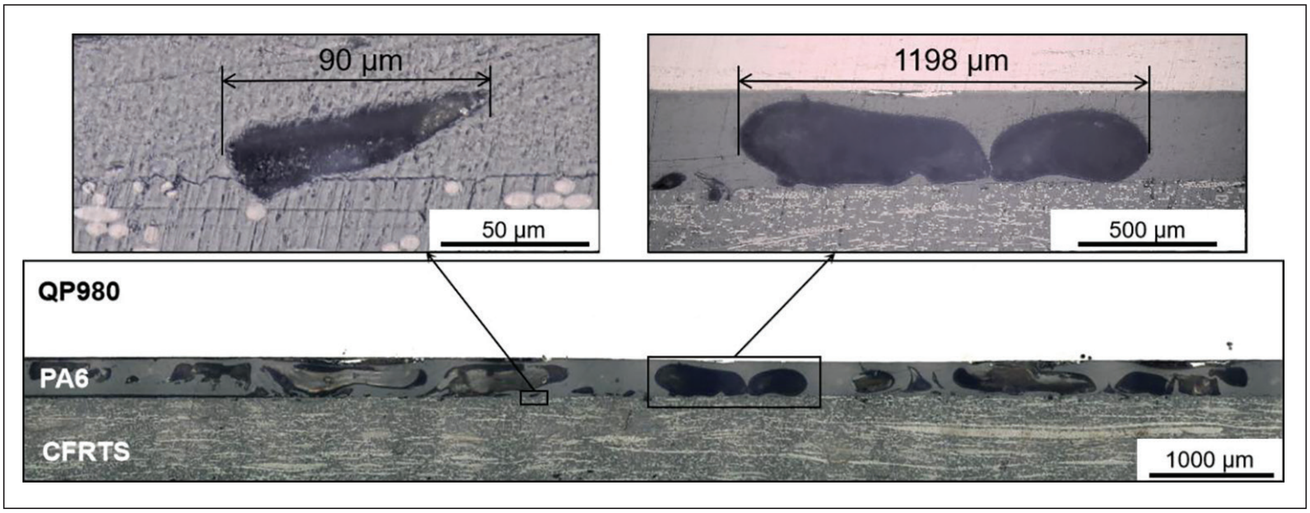

Fig. 4 — Porosities in the QP980/CFRTS joint (laser line energy of 120 J/mm and interfacial pressure of 0.2 MPa).

Materials and Methods

Materials

The CFRTS used in this experiment consisted of 63% epoxy resin and chopped carbon fiber. PA6, which has high mechanical strength, high impact toughness, and excellent fluidity, was adopted as the interlayer. The selected steel was QP980, the representative product of the third-generation advanced, high-strength steel for automobiles. As shown in Fig. 1, the specimen dimensions of the CFRTS/QP980 were 120 × 45 × 2 mm (4.72 × 0.47 × 0.08 in.), and the dimensions of the PA6 interlayer were 45 × 12 × 0.3 mm (1.77 × 0.47 × 0.01 in.). The material properties of the CFRTS and PA6 are shown in Table 1. Before the experiments, the surface of the QP980 steel was polished with #240 sandpaper to remove the oxide layer and impurities on the surface, after which the surface was cleaned with ethanol. The surface of the CFRTS was polished using #240 sandpaper to remove the moisture, release agent, and plasticizer to maintain constant surface quality.

Laser Joining Process

The epoxy resin of the CFRTS is nonfusible due to its thermosetting property, which is unable to be directly connected with metal by exposure to a laser beam. In the laser joining process, the thermoplastic interlayer must be added between the CFRTS and metal. In this study, the laser joining process of the QP980/CFRTS is schematically shown in Fig. 2. A layer of 0.3-mm-thick PA6 sheet was added between the QP980 and CFRTS, and then the laser was irradiated on the surface of the QP980. The laser radiation on the surface of the steel was converted into heat energy, which transferred to the PA6 layer. With the exposure of laser radiation and air convection, the PA6 layer experienced the melting, cooling, and solidification stages, which eventually generated an effective QP980 and CFRTS joint.

Table 1 — Mechanical Properties and Temperature Characteristics of PA6 and Epoxy Resin of CFRTS

Materials	Ultimate Tensile Strength (MPa)	Elongation at Fracture (%)	Density (g/cm^3)	Glass Transition Temperature (°C)	Melting Temperature (°C)	Pyrolysis Temperature (°C)
Epoxy resin	210	1.2	1.45	—	—	350
PA6	60	> 30	1.15	70	223	300

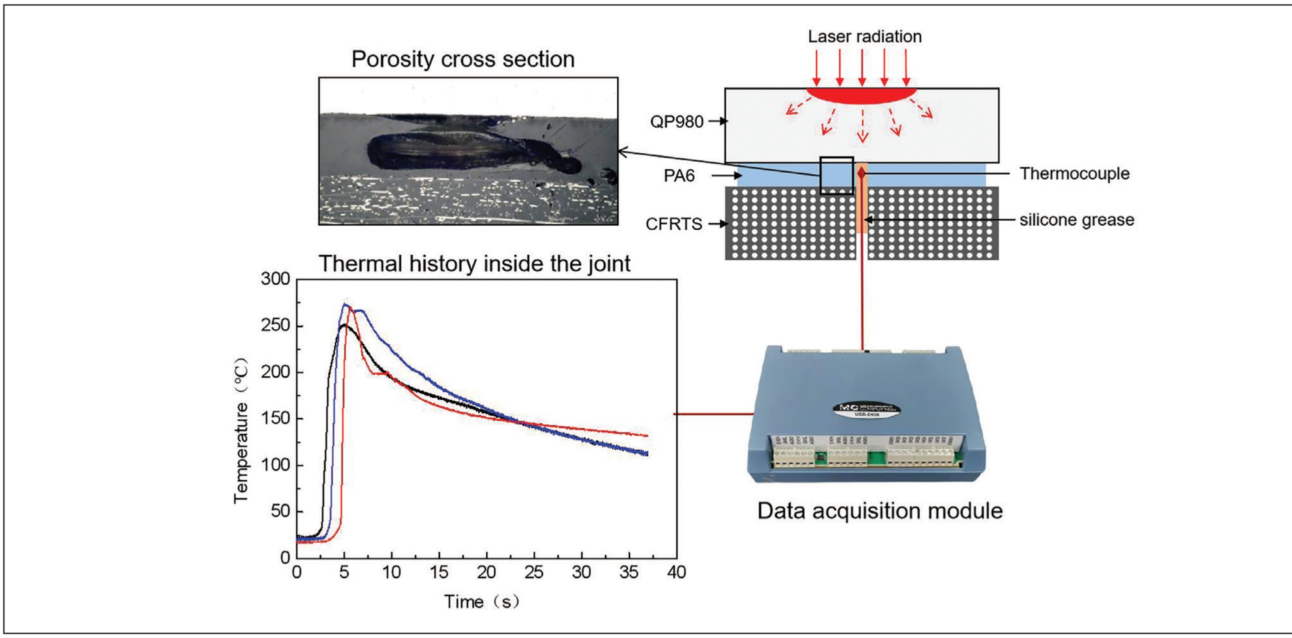

Fig. 5 — Schematic diagram and the results of the thermal history test.

A semiconductor laser (LDF 6000-30 from Laserline) with a wavelength of 940–1060 nm and maximum output power of 6600 W, was used. The spot profile was flat-topped, and the spot diameter was 0.6 mm (0.02 in.) on focus. After a series of preliminary experiments, it was found that heat conduction mode can produce a stable process when the defocusing amount was + 20 mm (0.79 in.) and the scanning speed was 5 mm (0.20 in.)/s. The line energy was varied by changing the laser power during the experiment.

Figure 3 shows the experimental setup of the laser joining process. A press plate was placed on the specimens, and pressure was applied on both sides of the press plate to fix the sample on the worktable. There was a strip groove in the middle of the press plate for laser irradiation. Spacers were placed on the CFRTS and under the QP980 to maintain the level and tightly fit the structure. A thin film pressure sensor for pressure measurement at the connection interface allowed the interfacial pressure of the QP980/CFRTS to be measured in the experiment.

Test and Analysis Methods

The lap shear tests of the specimens with different line energy were performed at room temperature by a universal testing machine (SUNS UTM5105), of which the load capacity was 100 kN and the cross head speed was 1 mm (0.04 in.)/min. To calculate the shear strength of the joint, the melting area of the PA6 was calculated as the connection area according to the fracture and cross-section morphology. The macroscopic morphologies of the cross section were observed and analyzed by an ultra-depth field microscope (UFM, VHX-6000 from KEYENCE Co.). The microscopic morphologies of the fractured surface were observed and analyzed by the Zeiss Merlin Compact scanning electron microscope (SEM).

Results and Discussion

Porosity Formation Mechanism

The effect of different laser line energies on the porosity formation of the QP980/CFRTS joint was investigated. The test results showed that if the PA6 interlayer melted, the porosities tended to be formed in the joint, as shown in Fig. 4. The porosity size was about 100 to 1000 microns, and it had a long strip and irregular shape. According to the existing research, two kinds of mechanisms of the porosity's formation have been reported. The mainstream view is that the epoxy resin or PA6 pyrolysis was induced by high temperature, which produced the gases, such as CO_2, CO, CH_4, and H_2O, entering the molten PA6 and forming bubbles (Refs. 6–12). Another view is that the molten PA6 shrank during the cooling and solidification stages (Refs. 8, 12), which led to the shrinkage cavity. The pyrolysis bubbles can be prevented by reducing the line energy, but the shrinkage defects cannot be eliminated with the same method.

To investigate the cause of the porosity formation, a thermal history test of the QP980/CFRTS joint was designed. As shown in Fig. 5, the thermocouple was embedded in the joint in the center of the laser scanning path and the thermocouple mounting hole was sealed with silicone grease. Through the data acquisition module, the temperature change of the joint during the laser joining process was measured in real time. To ensure accuracy, tests were repeated three times under the same laser parameters (the laser line energy of 120 J/mm). The results showed the peak value of the thermal history was lower than the pyrolysis temperature of the epoxy resin (350°C/662°F) and PA6 (300°C/ 572°F), which cannot cause the pyrolysis of the two resins. However, porosities were also formed in the joint. As a result, the formation of the porosities could not be attributed to the pyrolysis gas. The porosities in

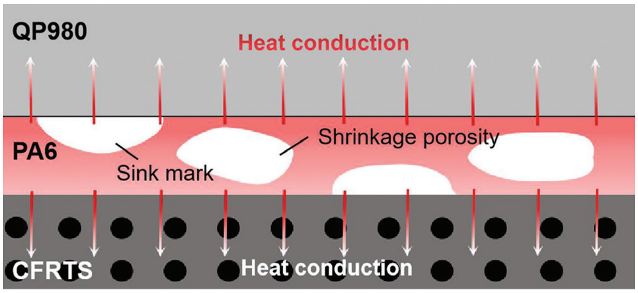

Fig. 6 — Schematic diagram of heat transfer during the solidification of the QP980/CFRTS joint.

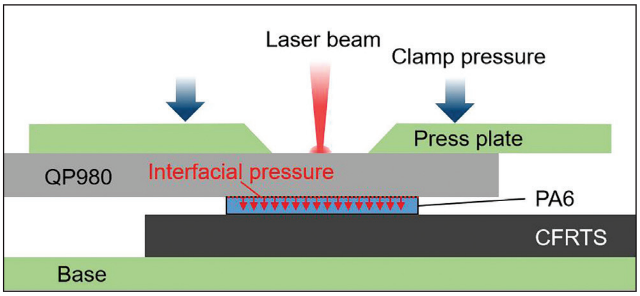

Fig. 7 — Diagram of interfacial pressure control.

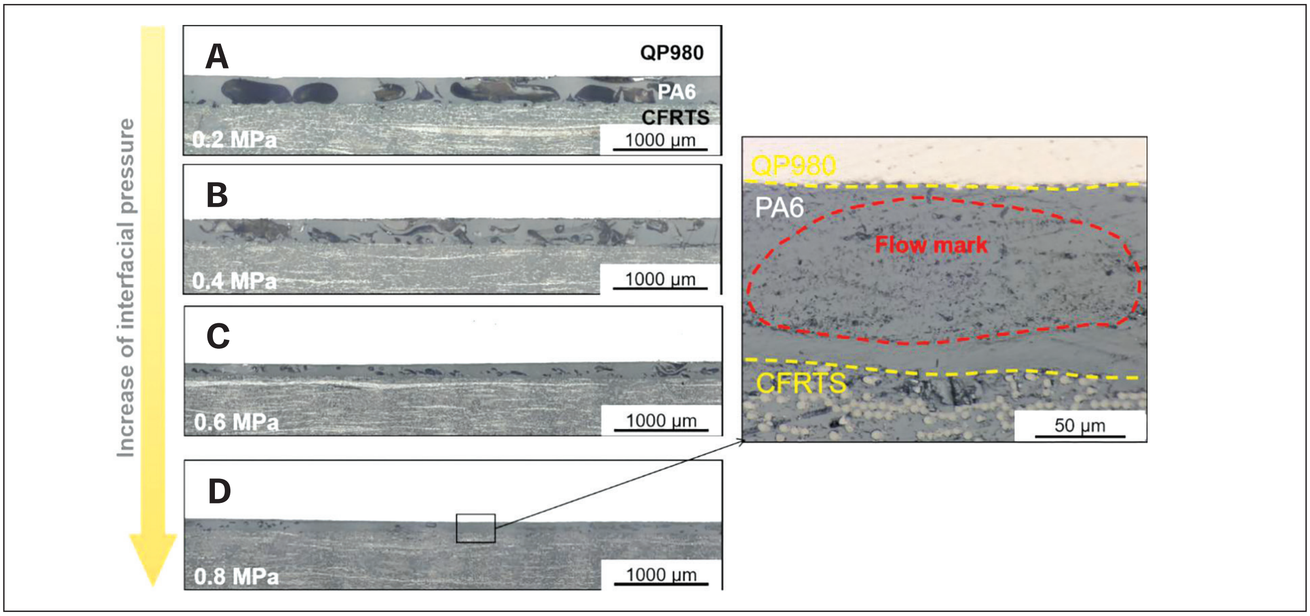

Fig. 8 — A cross-sectional view of QP980/CFRTS joints under the interfacial pressure: A — 0.2; B — 0.4; C — 0.6; D — 0.8 MPa.

Fig. 5 were long-shaped and irregular. Furthermore, they had a rough inner surface with protrusions and grooves, which are consistent with the characteristics of shrinkage defects formed under thermal shrinkage stress (Ref. 8). Therefore, the porosities in the QP980/CFRTS joint were regarded as shrinkage defects formed during the cooling and solidification stages of the PA6 interlayer.

During the solidification stage of the laser joining process, the shrinkage defects were inevitable due to the volume shrinkage of PA6. Figure 6 is a schematic diagram of the heat transfer of the QP980/CFRTS joint during solidification. The heat was rapidly transferred from the QP980 and CFRTS, so the internal and external cooling rates of PA6 were different. The molten PA6 near the interface of the QP980/PA6 and CFRTS/PA6 first formed a solidified layer, while the core layer was still in a molten state. At that moment, the core layer began to cool and shrink, which pulled the surface layer near the interface. If the interface bonding strength between the PA6 surface layer and the QP980 or CFRTS are not enough to resist the shrinkage force, the surface layer will be concave, resulting in sink marks. If the interface bonding strength are enough to resist the shrinkage force, shrinkage cavities start to form in the core layer (Refs. 13–16).

As long as remelting and solidification stages begin, shrinkage will occur. Shrinkage porosities reduce the effective connection area and generate stress concentration at the QP980/PA6 and CFRTS/PA6 interfaces, which is detrimental to interface joint strength.

Method for Eliminating Shrinkage Defects

The formation of shrinkage defects is directly related to holding pressure in the resin molding process (Refs. 13–19). A dynamical adjustment of the clamping pressure was designed in this study.

The clamping pressure was adjusted for the purpose of changing the interfacial pressure to investigate its effect on shrinkage porosities formation. The diagram of the interfacial pressure control is shown in Fig. 7. Based on the above experimental conditions (laser line energy of 120 J/mm and defocusing distance of 20 mm), the interfacial pressure was the only variable factor increasing from 0.2 to 0.8 MPa while

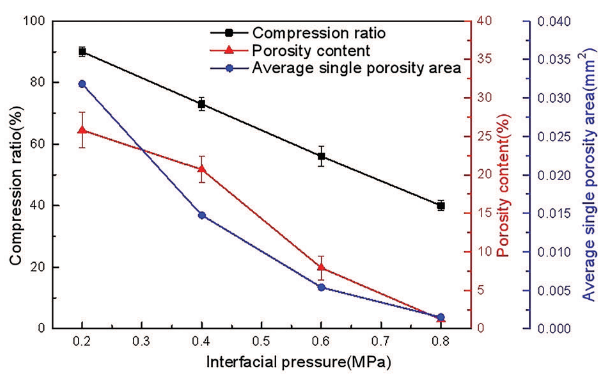

Fig. 9 — The effect of interfacial pressure on compression ratio and porosity content.

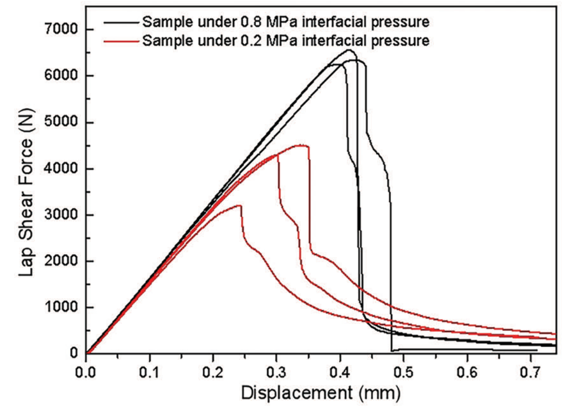

Fig. 10 — Force-displacement curves for lap shear tensile specimens of the QP980/CFRTS joints.

keeping the other joining parameters constant. The image processing method was used to identify the cross section of the joints and calculate the porosities number and its dimensions. Figure 8 shows the cross-sectional view of the QP980/CFRTS joint under different interfacial pressure levels, and Fig. 9 shows the effects of interfacial pressure on the compression ratios (the ratio of the thickness of the interlayer to the original thickness after laser joining) and the dimensions. Under high interfacial pressure, the compression ratio can be reduced from 90 to 40%. The porosity can be reduced from 25.8 to 1.2%. The average area of single porosity can be reduced from 0.0318 (4.93) to 0.0015 mm^2 (2.32 in.^{2}). The result indicates that the more compressed and filled molten PA6 becomes, the less shrinkage defects can be achieved with higher interfacial pressure. The wavy line texture shown in Fig. 8 is similar to the flow marks often seen in plastic injection molding. Many scholars believe the formation of wavy flow marks is caused by the instability of plastic melt flow (Ref. 20). Under the action of interfacial compressive stress, the plastic melt is disturbed along the thickness direction in the melting and solidification stages. Therefore, the wavy flow marks appear on the cross section of the joint. This phenomenon proved that the interfacial pressure has a significant effect on the formation of the interlayer.

Mechanical Performance

The mechanical performance of the joints was evaluated by a lap shear test under tensile loading. Figure 10 shows load-displacement curve of QP980/CFRTS laser joints under line energy of 120 J/mm. The results show that the average ultimate lap shear force of the joint under the interfacial pressure of 0.8 MPa was 6384N and the average shear strength was 18.06 MPa. The average ultimate lap shear force of the joint under the interfacial pressure of 0.2 MPa was 3999.3N and the average shear strength was 10.69 MPa. Therefore, increasing the interfacial pressure significantly eliminated the shrinkage defects, resulting in a 73.99% increase in the shear strength of the joint. At the same time, better uniformity also made the mechanical properties of the joint more stable under high interfacial pressure.

Fracture Morphology and Fracture Mode Analysis

Figure 11 shows the SEM images and 3D morphologies of the QP980/CFRTS joints' fractures. According to the fracture surfaces of the joints obtained under the interfacial pressure of 0.8 MPa, it is obvious that the PA6 interlayer was almost uniform and flat and adhered to the surface of CFRTS, and there were only a few traces of tensile deformation or stripped PA6. On the fracture side of QP980 steel, the completed surface, except for a small amount of PA6 debris, was observed. Overall, the fracture mode of the QP980/CFRTS joint under interfacial pressure of 0.8 MPa was the QP980/PA6 interface fracture, as shown in Fig. 12A.

Under interfacial pressure of 0.2 MPa, a large amount of PA6 attached to the fracture surfaces of the QP980 and CFRTS. The PA6 on the fracture surface of the CFRTS side was thin, and the surface of PA6 showed an irregular morphology of tensile deformation. However, there were a small amount of exposed CFRTS surface on the fractured surface, which could be the area where the interface of the CFRTS/PA6 did not connect due to the pull of the sink mark. The PA6 on the fractured surface of the QP980 side was thick, and a great number of pits could be observed. These pits were shrinkage defects after tensile fracture, but it is difficult to judge whether they were sink marks or shrinkage cavities. The tensile deformation of PA6 was distributed around the pits, which was due to the continuous extension of PA6 around the shrinkage defects during the lap shear test. The fracture mode of the QP980/CFRTS joint produced under interfacial pressure of 0.2 MPa was the PA6 cohesive fracture, as shown in Fig. 12B. From the above discussion, the elimination of shrinkage defects increases the effective load area of the PA6 interlayer, avoids stress concentration, and improves the overall tensile strength. Therefore, the fracture mode changes from cohesive fracture along the shrinkage defects

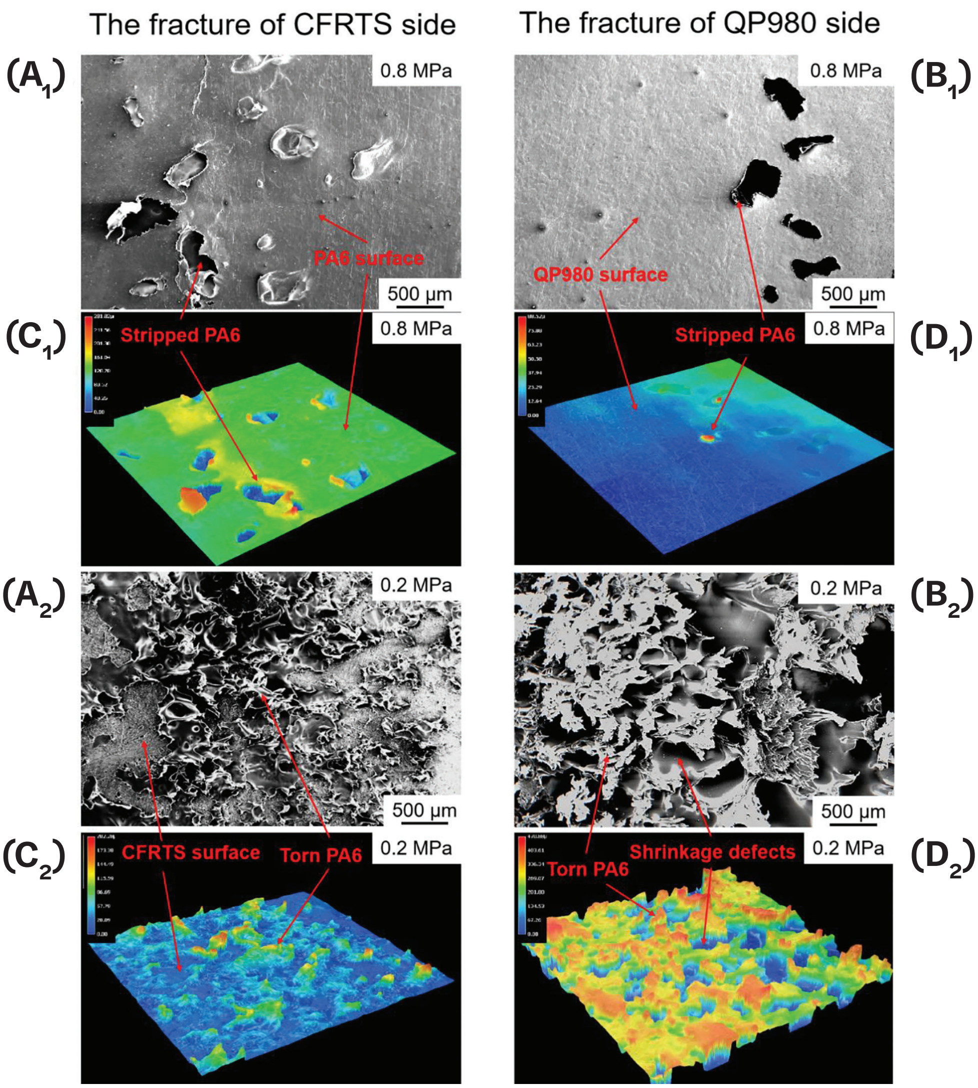

Fig. 11 — The effect of interfacial pressure on the fracture morphology; SEM images of fractures under 0.8 MPa pressure at the (A_1) CFRTS and (B_1) QP980 sides. 3D morphologies of fractures under 0.8 MPa pressure at the (C_1) CFRTS and (D_1) QP980 sides. SEM images of fractures under 0.2 MPa pressure at the (A_2) CFRTS and (B_2) QP980 sides. 3D morphologies of fractures under 0.2 MPa pressure at the (C_2) CFRTS and (D_2) QP980 sides.

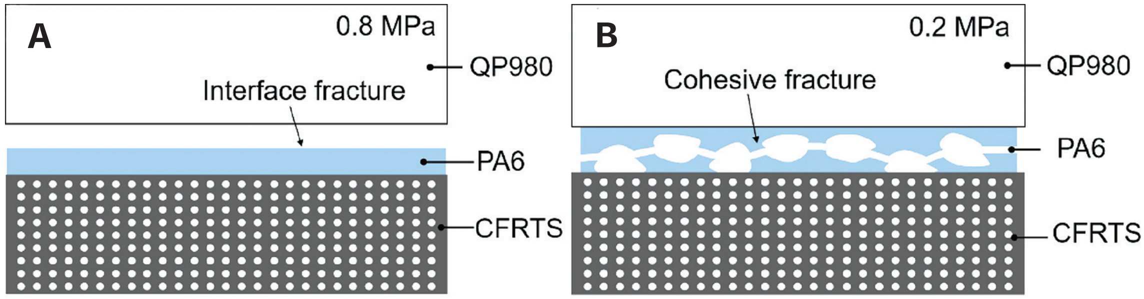

Fig. 12 — Fracture mode of joints under 0.8 (A) and 0.2 (B) MPa pressure.

of PA6 interlayer to QP980/PA6 interface fracture, which contributes to a significant improvement of the strength and stability of the joint.

Conclusion

In this paper, PA6 was adopted as an interlayer lying between CFRTS and QP980 steel to join two base materials via the laser joining process. The main conclusions are as follows:

1) The porosities that reduce the shear strength of QP980/CFRTS joints are mainly formed by PA6 solidification shrinkage rather than pyrolysis gas release.

2) By laser joining technology with a proposed high interfacial pressure, the molten PA6 was compressed, and the shrinkage defects were fully filled by surrounding liquid during the solidification stage, resulting in a decline of porosity from 25.8 to 1.2% and a reduction of the average single porosity area from 0.0318 to 0.0015 mm^2.

3) The elimination of shrinkage defects increases the effective load area of the PA6 interlayer, avoids stress concentration, enhances the tensile strength of the PA6 interlayer, and finally changes the fracture mode of the QP980/CFRTS laser joint from the cohesive fracture of the PA6 interlayer to the interface fracture of the QP980/PA6. The shear strength of the joint is significantly increased from 10.69 to 18.6 MPa by 73.99%.

Acknowledgments

The authors greatly thank the financial supports of Shanghai Municipal Economic and Informatization Commission [No. CXZX-2019-01] and Natural Science Foundation of Shanghai [20ZR1464300].

References

1. Jung, K. W., Kawahito, Y., Takahashi, M., and Katayama, S. 2013. Laser direct joining of carbon fiber reinforced plastic to aluminum alloy. *Journal of Laser Applications* 25(3). DOI: 10.2351/1.4794297

2. Tan, C., Su, J., Zhu, B., Li, X., Wu, L., Chen, B., Song, B., and Feng, J. 2020. Effect of scanning speed on laser joining of carbon fiber reinforced PEEK to titanium alloy. *Optics & Laser Technology* 129. DOI: 10.1016/j.optlastec.2020.106273

3. André, N. M., Goushegir, S. M., dos Santos, J. F., Canto, L. B., and Amancio-Filho, S. T. 2016. Friction Spot Joining of aluminum alloy 2024-T3 and carbon-fiber-reinforced poly (phenylene sulfide) laminate with additional PPS film interlayer: Microstructure, mechanical strength and failure mechanisms. *Composites Part B: Engineering* 94: 197–208. DOI: 10.1016/j.compositesb.2016.03.011

4. Jung K. W., Kawahito, Y., Takahashi, M., and Katayama, S. 2013. Laser direct joining of carbon fiber reinforced plastic to zinc-coated steel. *Materials & Design* 47: 179–188. DOI: 10.1016/j.matdes.2012.12.015

5. Jung, K. W., Kawahito, Y., and Katayama, S. 2013. Laser direct joining of carbon fibre reinforced plastic to stainless steel. *Science and Technology of Welding and Joining* 16(8): 676–680. DOI: 10.1179/1362171811Y.0000000060

6. Lin, J., Zhang, J., Min, J., Sun, C., and Yang, S. 2021. Laser-assisted conduction joining of carbon fiber reinforced sheet molding compound to dual-phase steel by a polycarbonate interlayer. *Optics & Laser Technology* 133. DOI: 10.1016/j.optlastec.2020.106561

7. Chen, Y. J., Yue, T. M., and Guo, Z. N. 2017. Laser joining of metals to plastics with ultrasonic vibration. *Journal of Materials Processing Technology* 249: 441–451. DOI: 10.1016/j.jmatprotec.2017.06.036

8. Tan, X., Zhang, J., Shan, J., Yang, S., and Ren, J. 2015. Characteristics and formation mechanism of porosities in CFRP during laser joining of CFRP and steel. *Composites Part B: Engineering* 70: 35–43. DOI: 10.1016/j.compositesb.2014.10.023

9. Tao, W., Su, X., Chen, Y., and Tian, Z. 2019. Joint formation and fracture characteristics of laser welded CFRP/TC4 joints. *Journal of Manufacturing Processes* 45: 1–8. DOI: 10.1016/j.jmapro.2019.05.028

10. Katayama, S., and Kawahito, Y. 2008. Laser direct joining of metal and plastic. *Scripta Materialia* 59(12): 1247–1250. DOI: 10.1016/j.scriptamat.2008.08.026

11. Jiao, J., Wang, Q., Wang, F., Zan, S., and Zhang, W. 2017. Numerical and experimental investigation on joining CFRTP and stainless steel using fiber lasers. *Journal of Materials Processing Technology* 240: 362–369. DOI: 10.1016/j.jmatprotec.2016.10.013

12. Zhang, Z., Tan, X. H., Zhang, J., and Shan, J. G. 2018. Suppression of shrinkage porosity in laser-joining of CFRP and steel using a laser surface modification process "Surfi-Sculpt ®". *International Journal of Adhesion and Adhesives* 85: 184–192. DOI: 10.1016/j.ijadhadh.2018.06.013

13. Pierick, D., Noller, R., Soc, P. E., and Plast, E. 1991. Effect of processing conditions on shrinkage. 252–258. DOI: 10.4028/www.scientific.net/KEM.501.294

14. Ansen, K. M. B., Van, D. J., and Husselman, M. 1998. Effect of processing conditions on shrinkage in injection molding. *Polymer Engineering and Science* 38: 838–846. DOI: 10.1002/pen.10249

15. Shen, C. Y., Wang, L. X., Cao, W., and Qian, L. 2007. Investigation of the effect of molding variables on sink marks of plastic injection molded parts using taguchi DOE technique. *Polymer-Plastics Technology and Engineering* 46(3): 219–225. DOI: 10.1080/03602550601152887

16. Gogos, C. G., Huang, C. F., and Schmidt, L. R. 1986. The process of cavity filling including the fountain flow in injection molding. *Polymer Engineering and Science* 26: 1457–1466. DOI: 10.1002/pen.760262016

17. Sundback, C., Hadlock, T., Cheney, M., and Vacanti, J. 2003. Manufacture of porous polymer nerve conduits by a novel low-pressure injection molding process. *Biomaterials* 24(5): 819–830. DOI: 10.1016/S0142-9612(02)00409-X

18. Beehag, A., and Ye, L. 1996. Role of cooling pressure on interlaminar fracture properties of commingled CF/PEEK composites. *Composites Part A: Applied Science and Manufacturing* 27(3): 175–182. DOI: 10.1016/1359-835X(95)00027-Y

19. Wakeman, M. D., Zingraff, L., Bourban, P. E., Månson, J. A. E., and Blanchard, P. 2006. Stamp forming of carbon fibre/PA12 composites — A comparison of a reactive impregnation process and a commingled yarn system. *Composites Science and Technology* 66(1): 19–35. DOI: 10.1016/j.compscitech.2005.06.001

20. Bogaerds, A. C. B. 2002. *Stability Analysis of Viscoelastic Flows*. Ph.D. dissertation, Eindhoven University of Technology. DOI: 10.6100/IR558902

JINYU BAI, **SHANGLU YANG** (*yangshanglu_lab@126.com*), **ZHE LIN**, and **QIAN YIN** are with Shanghai Institute of Optics and Fine Mechanics Chinese Academy of Sciences, Shanghai, China. **YANG** is also with the Center of Materials Science and Optoelectronics Engineering University of Chinese Academy of Sciences, Beijing, China.